THE DIRECTIVITY OF HIGH-ENERGY EMISSION FROM SOLAR FLARES: *SOLAR MAXIMUM MISSION* OBSERVATIONS

W. THOMAS VESTRAND, D. J. FORREST, AND E. L. CHUPP
Physics Department, University of New Hampshire

E. RIEGER
Max Planck Institute for Extraterrestrial Physics

AND

G. H. SHARE
E. O. Hulburt Center for Space Research, US Naval Research Laboratory
Received 1986 June 30; accepted 1987 May 14

ABSTRACT

The data base consisting of flares detected by the gamma-ray spectrometer (GRS) on board the *Solar Maximum Mission* (*SMM*) satellite is used to study the directivity of high-energy radiation. We present a number of observations that, altogether, strongly indicate that the high-energy emission from flares is aniso-tropic. They are the following: (1) the fraction of events detected at energies >300 keV near the limb is higher than is expected for isotropically emitting flares; (2) there is a statistically significant center-to-limb variation in the 300 keV to 1 MeV spectra of flares detected by the *SMM* GRS; (3) the 25-200 keV hard X-ray spectra measured during the impulsive phase by the *SMM* GRS show a center-to-limb variation; and (4) nearly all of the events detected at >10 MeV are located near the limb. We argue that if the emitting electrons are accelerated high in the solar atmosphere, then these observations are best explained by models in which nonthermal electrons radiate in a thick-target emission region lower in the atmosphere. To produce the observed center-to-limb variations, one needs an electron distribution that has an intensity which increases with angle from the outward normal. Candidate distributions are downwardly directed Gaussian beams and "pancake" distributions that peak in directions parallel to the photosphere. During the impulsive phase of the flare this nonthermal component seems to be visible down to energies less than 40 keV. These results imply that the procedure normally used to deduce the properties of flare-accelerated electrons from hard X-ray and gamma-ray observations can substantially underestimate the spectral hardness and number of high-energy electrons. Another consequence is that, on the average, disk flares should appear to be richer in nuclear emis-sion than limb flares.

Subject headings: gamma rays: general — Sun: flares — X-rays

I. INTRODUCTION

The directivity of radiation from flares can place important constraints on models of solar flares. Unfortunately, a single satellite cannot measure the directivity of radiation from a given flare because there is no straightforward independent measure of the flare's luminosity. To circumvent this problem, several groups have studied center-to-limb variations in flare frequency and flare spectra. The idea is that if the geometry of flares does not vary too markedly from flare to flare, then any variations with longitude on the solar disk will be due to an-isotropy of the flare radiation. The most ambitious studies employing this technique are the hard X-ray studies of Datlowe *et al.* (1977) and Kane (1974), whose data bases con-sisted of 148 events and 300 events from the satellites *OSO 7* and *OGO 5*, respectively. Both statistical studies concluded that at those energies (viz., ∼20 keV) the flare-frequency obser-vations were consistent with the hypothesis that the radiation was isotropic. On the other hand, Roy and Datlowe (1975) found that the spectra of *OSO 7* events showed a statistically significant center-to-limb variation. Specifically, they found that events near the limb had power-law spectra that on average were steeper than those of events on the disk by $\Delta p \approx 0.8$.

More recently, Kane *et al.* (1980) have tried to measure stereoscopically the directivity of radiation between 50 and 100 keV from individual flares. This was accomplished by compar-ing 50–100 keV fluxes from two spacecraft that observed flares from different viewing angles. While only three of the eight flares they studied had view angles that differed by more than 30°, the authors argued that all of the measurements were consistent with the hypothesis that the radiation is isotropic.

Compton backscattering of flare X-rays off the solar atmo-sphere complicates the interpretation of these hard X-ray observations. Several authors have shown that even substan-tial anisotropies in the primary radiation pattern can be "washed out" by Compton backscattering (Henoux 1975; Bai and Ramaty 1978; Langer and Petrosian 1977). At energies less than 100 keV this strong backscattering can make the flare radiation pattern appear isotropic even if the electron velocity distribution is directed strongly downward. As a consequence, studies at less than 100 keV are rather insensitive to an-isotropies in the energetic electron distributions.

In a related paper, Vestrand and Ghosh (1987*a*) developed diagnostics that measure the directivity of flare gamma rays and related the directivity to anisotropies in the angular dis-tribution of radiating electrons. In this paper we apply those diagnostics to flare observations by the gamma-ray spectrom-eter (GRS) on board the *Solar Maximum Mission* (*SMM*) satel-lite.

While we examine the 25–200 keV spectra of flares, our

study concentrates primarily on the directivity of flare radiation at energies >300 keV. Radiation at these energies is more likely to show evidence for directionality than at lower energies, because (1) the Compton reflectivity is much smaller and (2) the directionality of the bremsstrahlung cross section is more pronounced.

The paper is organized as follows: In § II we discuss the determination of flare parameters and present a list of the flares used in this study. In § III we analyze the position distribution of gamma-ray flares and show that we can rule out the hypothesis that the emission is isotropic. In § IV we show that this conclusion is reinforced by the observed difference in the spectral index distributions for limb and disk flares. Evidence for center-to-limb spectral variations at both hard X-ray and gamma-ray energies is presented. In § V we give evidence for a strong radiation anisotropy at energies >10 MeV. Some of the implications of these results are discussed in § VI.

II. THE GAMMA-RAY SPECTROMETER OBSERVATIONS

The flares used in this study were detected at energies higher than 300 keV by the *SMM* GRS. This energy is the threshold of the *SMM* GRS, which is a multicrystal NaI(Tl) scintillation spectrometer that provides a 476 channel pulse-height spectrum over the energy range 300 keV–9 MeV. The instrument also has a thick CsI(Na) crystal that is used in conjunction with the seven NaI crystals to form a high-energy detector. This high-energy detector is sensitive to neutrons with energies >20 MeV and can measure the photon spectrum between 10 MeV and 100 MeV. For a more detailed description of the instrument we refer the reader to Forrest *et al.* (1980).

Between 1980 February and 1986 February, 150 flares were detected at >300 keV by the *SMM* GRS. These flares were found by searching the data base both visually and by computer in the 300–800 keV energy band. Table 1 lists the gamma-ray flares (GRF) and their positions on the solar disk. The *SMM* GRS does not have sufficient spatial resolution to determine flare locations. Instead each position was determined by searching the NOAA *Solar-Geophysical Data* (1980–1986) reports for a coincident Hα flare and then assigning the Hα position to the GRF. Whenever more than one Hα flare showed a time coincidence, the position of the most significant flare, as measured by IAU importance class, was selected. This criterion was used because GRFs that are temporally isolated generally have high Hα importance. A total of 146 GRFs have been identified with Hα flares and have been assigned positions on the solar disk in this manner. In the entire data base, 73% of the Hα flares identified with GRFs have brightness maxima that are classified as brilliant, and 67% are classified as of importance class 1 or higher.

The first step in determining the spectral index for each flare was to correct the measured spectrometer counts by subtracting the background count spectrum. This background count spectrum depends on the satellite's geomagnetic cutoff rigidity and detector aspect angle during the flare. To determine the background, we obtain the count spectra at nearly identical cutoff rigidities and aspect angles for orbits on the day before and the day after the flare. These count spectra are then averaged together, and each is compared with the average count spectrum. If the average background gives an acceptable χ^2 fit to the measured spectrum for each of the background days, we use it as the background count spectrum for the flare. After the measured count spectrum is corrected by subtracting the background count spectrum, it is compared with the count spec-
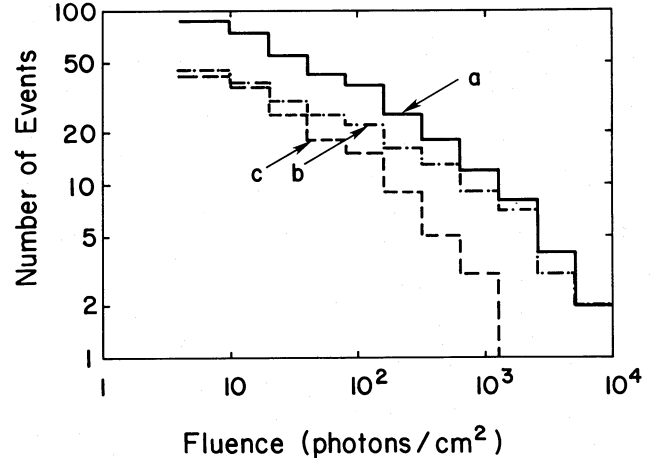

FIG. 1.—Histogram *a* shows frequency vs. fluence above 300 keV for all flares detected by the *SMM* GRS during the period 1980 February–1986 February. Histogram *b* is for flares at $\theta \geq 60°$, and histogram *c* is for flares at $\theta < 60°$.

trum produced by running a photon spectrum of the form AE^{-p} through the detector response function. Here A is essentially the differential intensity at 1 MeV. The best-fitting values of A and p are then determined by finding values that minimize the reduced χ^2 value for energies between 300 keV and 1 MeV. We were able to obtain spectral indices for 86 flares in this manner. Their spectral parameters are listed in Table 1. The remaining flares were too weak or had backgrounds that were too complicated to allow the determination of reliable spectral parameters.

The integral size distribution of the flares whose fluence could be reliably measured is shown in Figure 1. The number of events with >300 keV fluence that exceed S photons cm^{-2} is roughly proportional to $S^{-0.5}$ for fluences greater than 10 photons cm^{-2}. Deviations from this proportionality at fluences smaller than 10 photons cm^{-2} can be ascribed entirely to events lost in the instrumental background.

The *SMM* GRS has an auxiliary dector system designed to measure the X-ray continuum from flares. The system is composed of a pair of 8 cm^2 × 0.6 cm NaI(Tl) 4 channel X-ray detectors that are identical, except that one has an Al filter (X1) detector) and the other has an Al-Fe filter (X2 detector). The Al filter has a 50% transmission energy of ~13.5 keV, whereas the Al-Fe filter has a 50% transmission energy of ~30.8 keV. The X1 and X2 detectors have energy ranges of 14–114 keV and 14–200 keV, respectively. This arrangement allows one to determine which intense flares have spectral distortion from pulse pileup.

The positions of the identified GRFs (1980–1982) are shown in Figure 2. The figure shows that the distribution of positions has no statistically significant north-south or east-west asymmetry. Careful inspection of Figure 2 also indicates that there is an increase in the frequency of flares near the solar limb. A quantitative analysis of this apparent enhancement near the limb is the subject of the next section.

III. OBSERVED EVENT DISTRIBUTIONS

a) Introduction

Observations of flares at different positions on the solar surface give different views of the emitting region. Statistical studies of event distributions start by assuming that the radiation pattern is essentially the same for all flares. If this radi-

TABLE 1
Gamma-Ray Flares

Date	Time	Flare Position	GOES/Hα Class	θ	A cm⁻²MeV⁻¹	Index	Date	Time	Flare Position	GOES/Hα Class	θ	A cm⁻²MeV⁻¹	Index
1980 Mar 29	09:17:40	N27E42	C9.6/SB	53	...	...	1981 Sep 19	05:51:03	N08E46	M2.6/1B	46	...	...
1980 Mar 29	09:55:05	N07W10	M1.1/SB	17	0.98±0.07	−4.0±0.1	1981 Oct 7	22:56:15	S13E90	X3.6/1B	91	36.86±0.38	−2.8±0.1
1980 Apr 26	20:31:30	S17E61	M5.0/1B	61	...	...	1981 Oct 14	17:05:45	S06E86	X3.0/SB	87	305.36±0.85	−2.6±0.1
1980 Apr 28	20:39:55	S14W69	C9.9/SB	69	...	...	1981 Nov 1	18:12:49	S13E41	M1.6/1F	44	...	...
1980 May 9	07:12:17	S21W32	M7.2/1B	36	4.13±0.50	−2.5±0.2	1981 Nov 5	08:32:54	S10W12	M3.5/SB	18	...	...
1980 May 21	20:55:40	S14W15	X1.4/2B	19	3.32±0.29	−3.1±0.2	1981 Nov 12	16:00:40	N18W20	X1.2/1B	25	1.00±0.11	−3.8±0.2
1980 Jun 4	06:54:19	S14E59	M6.7/SB	60	14.53±0.34	−2.4±0.1	1981 Nov 22	03:22:26	S20W74	M1.2/1B	76	...	...
1980 Jun 6	11:42:32	S12E33	C3.6/SB	35	...	...	1981 Dec 7	14:50:40	S06E90	M1.9/SB	90	2.22±0.17	−2.8±0.2
1980 Jun 6	23:34:43	S13E35	C3.5/?N	37	...	...	1982 Jan 2	06:10:12	N19W88	M8.1/1B	89	7.22±0.33	−2.8±0.1
1980 Jun 7	01:17:16	N13W72	M2.5/SB	72	12.67±0.38	−2.6±0.1	1982 Jan 28	07:21:24	N07E46	M8.8/3B	48	7.78±0.25	−3.2±0.1
1980 Jun 7	03:11:57	N12W74	M7.6/SB	74	68.65±0.38	−3.0±0.1	1982 Feb 3	01:14:31	S15W29	X1.1/2B	30	...	...
1980 Jun 21	01:18:20	N20W90	X2.6/1B	89	1152.80±1.42	−2.5±0.1	1982 Feb 5	09:05:10	S14W44	M4.7/1B	44	4.68±0.23	−3.3±0.1
1980 Jun 29	10:41:40	S27W90	M4.2/1F	91	3.40±0.24	−3.0±0.1	1982 Feb 8	12:49:17	S13W88	X1.4/1B	87	182.17±0.68	−2.7±0.1
1980 Jul 1	16:26:52	S12W37	X2.5/1B	40	13.55±0.18	−3.4±0.1	1982 Feb 12	21:57:07	S12W22	M4.6/SB	22	...	...
1980 Jul 21	02:55:47	S15W60	M8.0/1B	63	32.49±0.44	−2.2±0.1	1982 Mar 26	05:48:05	S20E71	M2.2/SB	70	0.36±0.05	−4.5±0.2
1980 Aug 31	12:48:31	N12E28	M2.8/SB	28	1.91±0.26	−2.7±0.3	1982 Mar 30	05:36:25	N13W11	X2.8/3B	23	12.44±0.30	−3.3±0.1
1980 Sep 4	02:01:00	S07W18	M6.4/2B	23	...	...	1982 Apr 2	09:07:17	N09W62	M6.7/2B	64	14.42±0.29	−2.8±0.1
1980 Sep 8	05:03:50	N11E90	M3.4/1N	89	2.62±0.30	−2.5±0.2	1982 Apr 16	21:25:00	S04W90	M2.0/SN	90	...	...
1980 Oct 9	11:23:53	S13E51	M8.7/1B	54	...	...	1982 Jun 3	11:42:44	S09E72	X8.0/2B	72	2748.80±2.60	−2.0±0.1
1980 Oct 20	18:31:58	S17E45	M1.1/SB	50	...	...	1982 Jun 4	19:17:24	S10E53	M2.9/2B	54	1.62±0.14	−3.2±0.2
1980 Oct 23	10:34:01	N06W75	M1.0/SB	75	...	...	1982 Jun 5	01:28:47	S09E48	M6.2/1B	49	0.43±0.04	−4.5±0.2
1980 Nov 2	14:18:56	S20W59	C3.3/SB	63	...	...	1982 Jun 5	06:15:30	S10E40	X1.1/SB	41	3.02±0.30	−2.5±0.2
1980 Nov 5	22:32:50	N11E07	M4.0/1B	10	...	...	1982 Jun 6	16:39:00	S09E25	X12.0/3B	27	...	...
1980 Nov 6	03:44:07	S13E70	X9.0/2N	72	106.80±0.49	−2.9±0.1	1982 Jun 15	00:30:15	S12W90	M5.4/1B	90	19.93±0.34	−2.6±0.1
1980 Nov 7	02:04:12	N07W11	X2.7/2B	12	5.65±0.20	−3.2±0.1	1982 Jun 15	10:19:23	N13E47	X3.0/3B	48	8.10±0.32	−2.5±0.1
1980 Nov 8	14:52:30	S09E37	M2.4/1B	39	...	...	1982 Jun 15	15:11:34	S22E66	X1.3/2B	68	101.00±0.49	−2.8±0.1
1980 Nov 11	17:43:45	S11W71	M4.8/2B	72	3.68±0.26	−2.9±0.2	1982 Jun 20	01:13:22	N11W26	M1.0/SB	28	...	...
1980 Nov 12	04:48:32	N10W72	X2.5/2B	72	1.77±0.24	−2.8±0.3	1982 Jun 25	21:33:30	N17W61	M7.5/1B	62	4.58±0.41	−2.3±0.2
1980 Nov 15	15:42:27	S12W53	X1.9/1B	55	...	...	1982 Jun 26	00:48:00	N16W65	X1.9/2B	65	...	...
1980 Nov 16	09:04:20	N17W03	M8.7/2B	15	3.67±0.56	−2.2±0.3	1982 Jul 9	07:35:26	N17E73	X9.8/3B	73	319.21±0.81	−2.8±0.1
1980 Dec 17	08:45:14	N10E07	C7.6/SB	13	1.57±0.17	−2.7±0.2	1982 Jul 9	21:06:10	N18E79	M8.3/2B	78	78.50±0.51	−2.7±0.1
1980 Dec 18	19:21:17	N07W11	C5.7/SN	14	...	...	1982 Jul 9	22:50:45	N09E69	M1.9/SB	69	...	...
1980 Dec 23	21:15:03	NA	M3.0/-	...	...	...	1982 Jul 10	02:00:00	N18E68	M1.7/1B	68	...	...
1981 Jan 28	04:11:48	S13E55	M8.0/1B	55	9.49±1.31	−1.4±0.3	1982 Jul 10	03:16:43	N16E69	M1.2/SB	69	3.12±0.20	−2.7±0.2
1981 Feb 10	02:23:37	N09E14	C4.4/SN	21	...	...	1982 Jul 10	04:08:20	N16E69	M1.1/1B	69	1.95±0.22	−2.6±0.2
1981 Feb 10	03:20:09	S14W82	M1.2/SN	81	...	...	1982 Jul 10	08:30:44	N16E64	M2.4/1F	64	18.11±0.67	−3.1±0.1
1981 Feb 17	21:46:02	N20W20	X1.0/1B	33	1.74±0.13	−3.6±0.1	1982 Jul 11	06:36:53	N15E53	C9.9/1N	53	...	...
1981 Feb 20	06:44:58	N19W50	X2.4/2N	56	...	...	1982 Jul 17	02:03:00	N11W34	M8.5/1B	34	...	...
1981 Feb 24	00:10:27	S13E86	M5.2/SB	85	1.05±0.11	−3.4±0.2	1982 Jul 19	01:00:21	N20W45	X1.2/1B	46	7.56±0.21	−3.1±0.1
1981 Feb 24	19:36:11	S14E75	X1.4/2B	74	3.75±0.27	−2.9±0.2	1982 Jul 20	04:17:15	N22W59	M3.9/SN	60	7.17±0.23	−2.7±0.1
1981 Feb 26	14:24:39	S12E53	X1.8/SB	52	9.89±0.21	−3.3±0.1	1982 Jul 20	21:54:00	N20W69	M2.1/1B	69	...	...
1981 Mar 23	06:55:37	N10W52	M8.5/2N	55	3.25±0.24	−3.1±0.2	1982 Jul 21	18:22:41	N23W88	M3.4/SN	86	...	...
1981 Apr 1	01:33:04	S43W52	X2.3/3B	58	176.99±1.48	−2.5±0.1	1982 Jul 22	05:12:19	N22W90	M2.0/1N	88	9.50±0.32	−2.5±0.1
1981 Apr 2	11:04:53	S43W63	X2.2/1N	66	...	...	1982 Aug 8	02:03:56	S09W65	M7.2/1B	67	17.89±0.35	−2.8±0.1
1981 Apr 10	16:46:30	N07W36	X2.3/2B	38	24.33±0.28	−3.1±0.1	1982 Nov 22	12:23:12	S10W33	M2.0/2B	35	1.37±0.08	−3.3±0.1
1981 Apr 14	23:39:27	N13E73	M3.4/1N	75	2.07±0.28	−2.8±0.3	1982 Nov 23	13:45:40	N10W45	M1.2/3N	46	...	...
1981 Apr 15	06:43:15	N21W69	M1.8/1N	73	...	...	1982 Nov 25	04:14:03	S10W75	M2.4/1B	76	...	...
1981 Apr 18	10:49:20	NA	X1.0/-	...	...	...	1982 Nov 26	02:29:04	S11W87	X4.5/2B	87	136.47±0.64	−2.9±0.1
1981 Apr 26	11:44:05	N15W74	X1.2/2N	76	14.79±0.27	−3.8±0.1	1982 Dec 7	23:40:00	S19W79	X2.8/1B	80	1511.39±1.84	−3.0±0.1
1981 Apr 26	17:39:12	N14W79	- /SN	81	...	...	1982 Dec 13	03:24:32	S09E51	M8.3/2B	51	...	...
1981 Apr 27	08:03:28	N16W90	X5.5/1N	91	310.50±1.17	−2.7±0.1	1982 Dec 15	16:30:44	S10E15	X5.0/2B	17	22.48±0.23	−3.6±0.1
1981 May 4	08:38:08	N15E18	M9.0/1B	26	3.55±0.18	−3.7±0.1	1982 Dec 17	01:48:29	S10W03	M4.8/1B	9	...	...
1981 May 13	04:12:00	N09E58	X1.5/3B	59	14.75±0.37	−3.2±0.1	1982 Dec 17	18:56:44	S08W21	X10.1/3B	22	25.58±0.38	−2.7±0.1
1981 Jul 18	12:22:46	N07W18	C9.6/SF	18	...	...	1982 Dec 18	08:21:43	S10W20	X1.1/2B	22	1.50±0.16	−3.1±0.2
1981 Jul 19	05:33:20	S09E68	X2.7/2B	69	10.11±0.64	−2.2±0.2	1982 Dec 29	06:44:10	S13W12	X1.9/2B	16	14.45±0.17	−3.8±0.1
1981 Jul 19	05:58:44	S28W56	X2.7/2B	63	39.21±0.32	−3.3±0.1	1982 Dec 30	01:42:35	S13W22	M7.1/2B	24	1.49±0.19	−2.8±0.2
1981 Jul 26	04:10:43	S13E31	M2.3/1N	36	...	...	1983 Feb 3	06:03:19	S19W08	X4.1/1B	15	68.04±0.46	−3.4±0.1
1981 Jul 26	08:05:41	S14E30	X1.0/2B	36	0.51±0.07	−3.6±0.2	1983 April 27	02:54:00	S17E23	M1.1/1N	26	...	...
1981 Jul 26	13:53:18	S15E29	X3.5/2B	35	1.89±0.14	−3.1±0.2	1983 April 28	10:49:00	S03E24	M1.2/1B	24	...	...
1981 Jul 28	20:09:37	S09W18	M3.4/1B	23	2.37±0.27	−3.1±0.2	1983 May 7	22:16:36	S29E66	X3.1/2B	67	334.68±0.95	−2.5±0.1
1981 Jul 31	05:55:36	S13W41	C8.5/1N	45	...	...	1983 May 9	23:04:17	S29E41	X2.4/2B	47	45.41±0.48	−2.9±0.1
1981 Aug 10	06:58:52	S13W15	M4.8/1B	25	...	...	1983 May 25	09:52:00	N A	M2.2/	...	...	...
1981 Aug 30	09:09:35	S12E80	M2.1/1N	82	...	...	1983 Jun 9	21:58:00	S08E23	M1.8/SB	24	...	...
1981 Sep 5	06:59:34	N08E68	C5.9/SN	67	...	...	1983 Jun 25	20:50:00	S07E89	M4.0/SN	89	...	...
1981 Sep 6	00:01:07	S12W66	M8.1/1N	68	2.74±0.32	−3.1±0.2	1983 Jun 26	14:08:00	S13E76	M7.0/2B	77	...	...
1981 Sep 7	05:10:40	N09E45	M9.5/1N	45	...	...	1984 Apr 24	23:59:42	S11E45	X13.0/3B	45	970.14±1.48	−2.6±0.1
1981 Sep 7	22:22:51	N11W29	M4.2/SB	29	5.77±0.28	−2.9±0.1	1984 May 5	18:09:50	S11W91	M7.5/?	90	44.26±1.17	−2.2±0.1
1981 Sep 10	07:28:12	S11W70	C6.7/1N	72	...	...	1984 May 19	23:43:00	...	...	...	...	...
1981 Sep 10	09:38:43	N07E04	M8.4/2B	4	...	...	1984 May 20	05:40:00	S11E63	M5.4/1N	63	...	...
1981 Sep 15	21:13:57	N05W82	X2.3/2N	82	6.20±0.33	−2.6±0.1							

TABLE 1—Continued

Date	Time	Flare Position	GOES/Hα Class	θ	A cm^{-2}MeV^{-1}	Index
1984 May 20	21:53:29	S08E52	C5.7/SN	52	0.31±0.03	-4.5±0.2
1984 May 21	02:19:00	S09E52	M5.7/SN	52	...	...
1984 May 22	14:56:57	S09E26	M6.3/2B	27	0.30±0.03	-4.4±0.2
1984 Nov 10	20:02:00	N17E06	M3.7/1B	15	...	...
1985 Jan 21	23:58:19	S10W40	X4.7/1N	40	19.82±0.22	-3.6±0.1
1985 Apr 24	09:28:53	N05E24	X1.9/2B	26	120.80±1.00	-2.7±0.2
1985 Jul 2	21:20:00	S14E57	M4.5/2B	60	...	...
1986 Feb 4	07:35:36	S04E21	X3.0/3B	21	16.98±0.20	-3.7±0.1
1986 Feb 4	10:24:13	S03E66	M6.4/2N	66	39.19±0.51	-2.8±0.1
1986 Feb 6	06:20:33	S07W02	X1.7/2B	2	72.54±0.29	-3.8±0.1
1986 Feb 14	09:10:00	N01W76	M6.4/1B	76	...	...

ation pattern is anisotropic, then the apparent brightness of the flare and hence its detectability above a fixed instrumental threshold will vary with solar longitude. Variations in the flare frequency with longitude can therefore be interpreted as radiation directivity.

In our study we examine variations in flare frequency with heliocentric angle. The heliocentric angle, θ, is defined by the angle between the Earth-Sun line and the normal to the solar surface at the flare position (see Appendix B). The advantage of using heliocentric angle instead of longitude is that one does not implicitly assume that the flare occurred at the solar equator. This distinction will be important in the next section, where we study center-to-limb spectral variations.

Vestrand and Ghosh (1987a) show that the fraction of events with $\sin \theta > 0.9$, f_L, is a practical indicator of radiation directivity that is also relatively insensitive to the details of the flare latitude distribution. In this section we use the f_L diagnostic to study the position distribution of gamma-ray flares as well as several control samples.

b) Control Distributions

As a preliminary test of our analysis procedure we used data sets composed of GOES flares, HXRBS flares, and Hα flares to form control distributions. The flares in these classes are believed to have isotropic or nearly isotropic radiation patterns. They should, therefore, give position distributions consistent with that predicted for isotropic emission.

In order to determine the position distribution for flares, detected by the ion chambers on the Geostationary Operational Environmental Satellites (GOES), all events with GOES class M2.5 or higher were tabulated from the NOAA Solar-Geophysical Data reports for the period from 1980 February to 1986 February. Nearly 70% of all events detected at >300 keV are associated with events on this list. The position distribution was formed from only that subset of the events that occurred when the GRS was capable of detecting a coincident event. For example, GOES events that occurred while the SMM GRS was not observing the Sun, because of Earth occultation or while
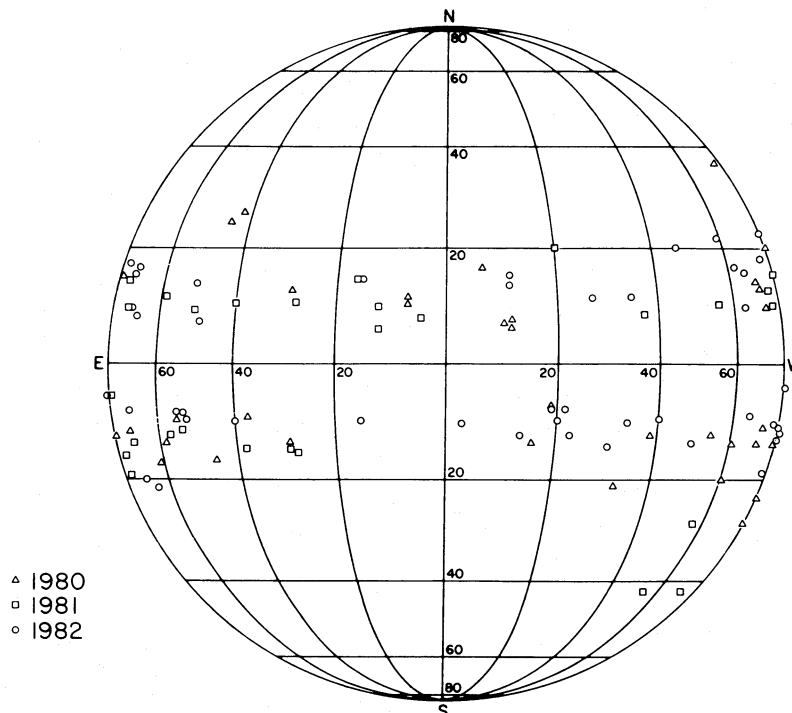

FIG. 2.—Positions of Hα events associated with flares detected by the SMM GRS at 300 keV during the period 1980 February–1982 December

the satellite was in the South Atlantic Anomaly, were eliminated from the data set. A subset of 233 *GOES* events remained after the events were culled.

If the flare radiation pattern is isotropic, then about 29.5% of the flares should have heliocentric angles θ such that $\sin \theta > 0.9$ (Vestrand and Ghosh 1987a). The flare radiation measured by the *GOES* satellite at energies between 1.3 and 12 keV is believed to be of thermal origin and should have an essentially isotropic radiation pattern. Therefore, in a sample of N *GOES* flares, we expect $0.295N$ events at $\sin \theta > 0.9$. The corresponding binomial uncertainty is $\sigma = 0.456N^{1/2}$ events. In the sample of 233 events we expect 68.74 ± 6.96 at positions with $\sin \theta > 0.9$. A total of 68 events were detected at $\sin \theta > 0.9$. The observed *GOES* distribution is therefore completely consistent with the Monte Carlo results for the isotropic radiation pattern.

Flares detected by the hard X-ray burst spectrometer (HXRBS) on board the *SMM* satellite (Dennis *et al.* 1986) were also used as a control distribution. All *SMM* HXRBS events that were detected between 1980 February and 1986 February with peak count rates greater than 10^3 counts s^{-1} comprise the sample of 424 events. The average energy of the detected photons is about 40 keV. At these energies Compton backscattering is so strong that even if the distribution of radiating electrons is highly anisotropic, the radiation pattern observed at the Earth will appear to be nearly isotropic (e.g., Bai and Ramaty 1978). If the radiation pattern is isotropic, then the predicted number of flares at $\sin \theta > 0.9$ is 125.08 ± 9.39 events. A total of 110 events were detected at $\sin \theta > 0.9$. The fraction of limb events is therefore slightly smaller than predicted but is still consistent with the Monte Carlo results for isotropic emission.

As a final control group, the distribution of Hα flares with importance 1F or higher were examined. The flare positions were obtained from the comprehensive reports distributed by the NOAA *Solar-Geophysical Data* (1980–1986) reports. Flares for the period 1980 February 15 to 1981 May were tabulated and selected to eliminate flares that occurred when the *SMM* GRS was not capable of detecting a coincident event. The final data set comprised 439 flares. The expected number of events at $\sin \theta > 0.9$ is 129.51 ± 9.56 events. The number of flares detected at $\sin \theta > 0.9$ is 118. Again, the fraction of limb events is slightly smaller than predicted by the Monte Carlo calculation for isotropic emission.

The slight limb deficiency found in the HXRBS and Hα control samples is probably the result of the nonuniform Hα visibility on the solar disk. It is well known that the visibility function of Hα flares decreases at large heliocentric angles (e.g., Smith and Smith 1963). Since the positions of flares detected at high energies are assigned by association with Hα flares, high-energy flares that occur near the limb are more likely to have an undetermined position or to be incorrectly associated with disk Hα flares.

c) *Gamma-Ray Flare Distribution*

In contrast to the three control samples, the events detected by the *SMM* GRS show a significant excess in the number of events near the limb. Of the 150 gamma-ray flares detected, a total of 146 have identified positions. If the flares emit isotropically, one would expect 43.1 ± 5.5 events to have heliocentric angles such that $\sin \theta > 0.9$. A total of 57 events were detected at $\sin \theta > 0.9$. There is, therefore, a 2.5 σ excess in the number of observed limb events. Thus we can formally reject
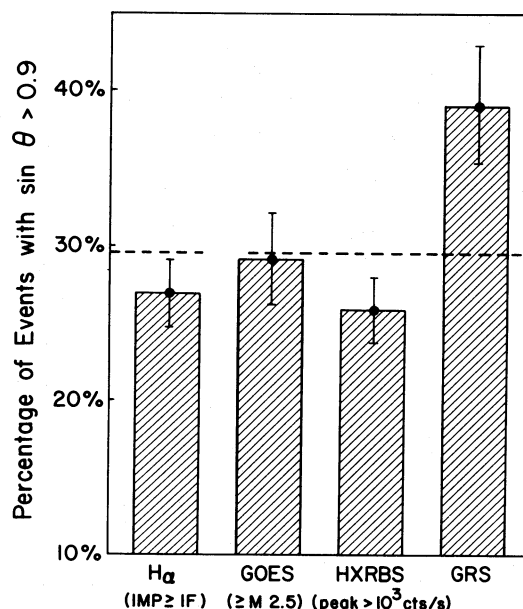

FIG. 3.—Fraction of events, f_L, occurring at heliocentric angles such that $\sin \theta > 0.9$. Shown are the results for Hα, *GOES*, *SMM* HXRBS, and *SMM* GRS samples that have been culled down to the subsets of events that occurred when the *SMM* GRS was capable of detecting a coincident event.

the hypothesis that the gamma-ray radiation pattern is isotropic at the 99% confidence level. Since upward beaming of the radiation reduces the fraction of limb events below the isotropic value, we can reject it at a significantly higher confidence level. Figure 3 shows the percentage of limb events found in the three control samples and the GRF sample. It clearly shows that there is a significant enhancement in the number of GRFs near the limb.

By comparing the observations with the Monte Carlo simulations, we have implicitly assumed that the position of each event is completely unrelated to the preceding event. However, a large fraction of the observed GRFs are associated with active regions that produced at least one other event. We therefore examined the possibility that the position distribution is systematically biased by these prolific active regions. To test this hypothesis, the GRFs were divided into two classes: (*a*) those that are associated with active regions that produced at least one other GRF and (*b*) those that are the only GRFs produced by the associated active region. The position distributions for these two classes were then formed and checked against one another using the Kolmogorov-Smirnov test (Lehmann 1975). The two samples were found to satisfy the null hypothesis that both were drawn from the same distribution. Prolific active regions therefore do not seem to significantly bias the event position distribution. Furthermore, if event clustering did produce the GRF limb enhancement, then the control samples should also exhibit the limb enhancement. No enhancement was found for any of the control samples.

A possible explanation for the excess in the fraction of gamma-ray events at $\sin \theta > 0.9$ is that the sample is contaminated by a number of events that are actually beyond the limb. One might argue that the gamma-ray emission is isotropic and that the limb excess is due to events that are beyond the limb but associated with the top parts of Hα flares. However, there are several arguments that show that this explanation is unlikely. They are listed below.

1. The HXRBS and *GOES* control samples do not show a limb enhancement. To compare with the gamma-ray sample, both control samples were limited only to relatively large events. Specifically, only HXRBS events with peak count rates greater than 1,000 counts s⁻¹ and *GOES* events of class M2.5 or higher were included in the samples. These size thresholds were selected to be comparable to the threshold for detection of gamma-ray flares. For example, roughly 70% of the gamma-ray events are associated with *GOES* events of class M2.5 or higher. At the energies where HXRBS and *GOES* events are identified the flare radiation patterns are believed to be nearly isotropic. The potential for detecting HXRBS events beyond the limb is comparable to or greater than the potential for detecting beyond-the-limb GRFs. (The attentuation constant is roughly 50% larger at 40 keV than it is at 300 keV. However, the height of the 40 keV emission region is likely to be greater because the range of the electrons that generate the bulk of the emission at those energies is roughly 1.5 orders of magnitude smaller.) Neither the HXRBS sample nor the *GOES* sample shows a limb enhancement that can be attributed to contamination by beyond-the-limb events.

2. One can also demonstrate quantitatively that beyond-the-limb events are not a likely source of the limb excess. Suppose that the excess of 14 events found at $\sin \theta > 0.9$ is due to beyond-the-limb but isotropically emitting events. Then all events must be essentially unattenuated to roughly 7° past the limb. However, temporal and spectral variability observations constrain the number density in the gamma-ray production region to be greater than 10^{12} cm⁻³ (see, e.g., Chupp 1984). This density constraint restricts the interaction region to a height of less than 1500 km above the photosphere. Using this height as an upper limit to the height of the production region, one can then calculate the attenuation of 300 keV emission for various angles beyond the limb. We find that emission from a height of 1500 km is attenuated by a factor of 20 even if the region is only 3° past the limb (see Appendix A). Beyond-the-limb events are therefore unlikely to be entirely responsible for the excess in GRFs with $\sin \theta > 0.9$.

Three of the limb events have heliocentric angles that place them beyond the limb. Taking only this result into account, the statistical significance of the limb excess should be reduced to about 2.2 σ. On the other hand, the reduced visibility of Hα events near the limb may have led to the misidentification of a few limb events as disk events or to the failure to obtain positions for a few limb flares (two *SMM* GRS flares do not have associated Hα positions). If only this bias is corrected for, then the significance of the excess should be raised to about 3 σ. The control samples seem to argue that the second effect is more important than the first. Since both effects should be of comparable magnitudes and tend to cancel one another, we have neglected them in our analysis.

A more likely explanation for the overabundance of GRFs at large heliocentric angles is that the γ-ray emission from flares is not isotropic. Possible radiation patterns include downwardly directed and tangentially directed distributions. To fix ideas, we assume that the radiation pattern is a downwardly directed Gaussian. One can show that the fraction of limb events that can be detected above the threshold of the *SMM* GRS increases as the width of the downwardly directed Gaussian decreases. To estimate the directivity of the radiation, we compared the observed limb fraction with the results from Monte Carlo simulations for various Gaussian beam patterns given in Vestrand and Ghosh (1987a). If the electron distribution is a downwardly directed Gaussian, then to produce the observed limb fraction $f_L = 0.39$, one must have a half-width at half-maximum of $\varphi_{1/2} \sim 75°$.

IV. SPECTRAL INDEX VARIATIONS

In the preceding section we argued that the increase in the frequency of GRFs at the limb is a result of the directivity of flare radiation. Since Compton backscattering of isotropic photon emission can introduce only a relatively small anisotropy (e.g., Bai 1977), the directivity of the flare radiation must be generated by an anisotropy in the velocity distribution of the radiating electrons. Such an anisotropy will produce another potentially observable feature, namely, the spectra of the radiation should vary with viewing angle. This spectral variation is produced by the fact that the bremsstrahlung is more strongly directed along the electron velocity vector at higher energies. Consequently, the photon spectrum softens in directions away from the direction of maximum electron flux.

a) Gamma-Ray Observations

To test the gamma-ray data for a center-to-limb spectral variation, we divided the flare sample into two subsets according to heliocentric angle (1) those at $\theta < 60°$ and (2) those at $\theta > 60°$. Figure 4 shows the histogram of the power-law spectral indices measured between 300 keV and 1 MeV for flares in each subset. The shape of the histograms are similar, but the average limb event seems to be harder than the average disk event. To test the distributions against one another, we again used the Kolmogorov-Smirnov test. The test assigns only one chance in 10^4 to the possibility that both distributions are drawn from the same parent distribution. The spectral index distributions for limb and disk GRFs are therefore significantly different.
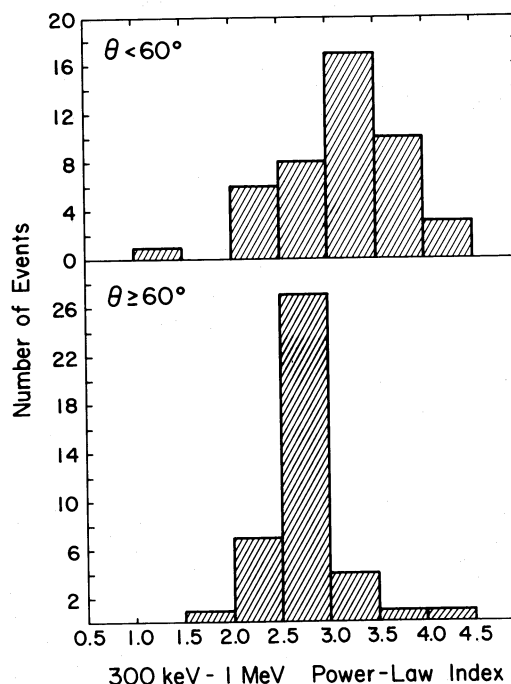

Fig. 4.—Histograms of power-law indices that provide the best fit to the *SMM* GRS measurements between 300 keV and 1 MeV. The distributions are shown for limb ($\theta > 60°$) and disk ($\theta < 60°$) samples.
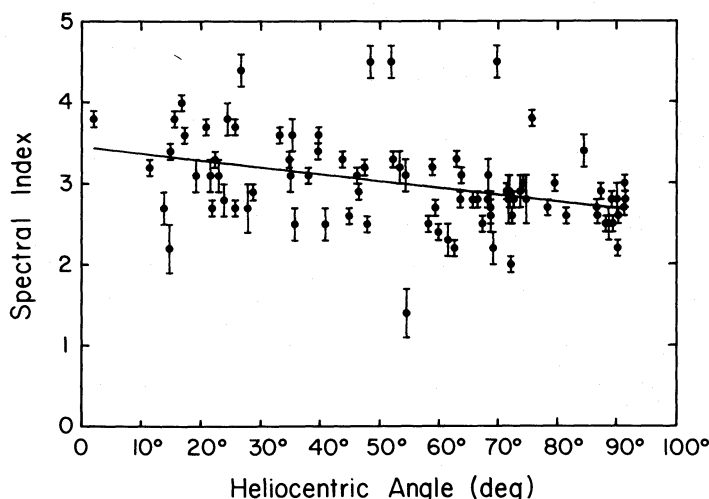
Fɪɢ. 5.—Best-fit 300 keV–1 MeV power-law indices versus heliocentric angle. The line providing the least-squares fit to the data is also plotted.

To obtain a more quantitative measure of this spectral variation, we compared the mean spectral indices for the limb and disk samples. Using the data listed in Table 1, we found that the 44 flares at $\theta < 60°$ have a mean spectral index $p_{disk} = 3.17 \pm 0.09$. The 42 flares with measured spectral indices that occurred at $\theta > 60°$ have a mean spectral index $p_{limb} = 2.80 \pm 0.06$. The spectra of limb flares therefore tend to be harder than those of disk flares by $\Delta p = 0.37 \pm 0.11$. In other words, the 300 keV–1 MeV spectra of flares detected by the *SMM* GRS show a limb spectral hardening at the 3.4 σ level.

The power-law indices and heliocentric angles of the flares detected by the *SMM* GRS are plotted in Figure 5. To guide the eye we have also plotted the line that provides the least-squares fit to the data: $p = 3.5(\pm 0.5) - 0.0086(\pm 0.0023)\theta$. From the figure one can see that the mean spectrum hardens with increasing heliocentric angle. It is also clear that at a given heliocentric angle the distribution of possible spectral indices is broader than the errors associated with the measurements. This, of course, indicates that there is an intrinsic spread in flare spectral indices.

b) Hard X-Ray Observations

If the emitting electrons are anisotropic, then there should also be a center-to-limb variation in the spectral hardness of hard X-rays from flares. To test for this variation we examined the 25–200 keV spectra derived from the hard X-ray detectors of the *SMM* GRS experiment. From 1980 February to 1982 December, 99 flares were detected with nominal peak rates in X2 of more than 1000 counts s^{-1}. A total of 31 of the larger events were removed from this sample because of clear evidence for pulse pileup in detector X1 or other instrumental effects. For the remaining events the hardness of the flare spectrum was characterized by the index of the power-law photon spectrum which gave the best agreement with the counting measurements of the eight independent X-ray channels.

To minimize spectral contamination by thermal X-ray emission, care was taken to accumulate the spectra only over time intervals that correspond to the impulsive phase at higher energies. For flares detected at energies greater than 300 keV, this interval was defined by the time profile at 300 keV. For those flares that were not detected at 300 keV, we used the time profile of the 56–200 keV count rate as measured by X-ray detector X2. The justification for this procedure is that when

both count rates are measured, the 56–200 count rate in detector X2 is well correlated with the 300 keV count rate.

The 25–200 keV spectral index distributions for events at $\theta < 60°$ and $\theta > 60°$ are shown in Figure 6. Again, the flares near the limb tend to have harder spectra than those on the disk. The 45 disk events have a mean power-law index of $p = 4.22 \pm 0.13$. The 27 limb events have a mean power-law index of $p = 3.71 \pm 0.16$. The hard X-ray events that occur near the limb therefore tend to be harder than disk flares by
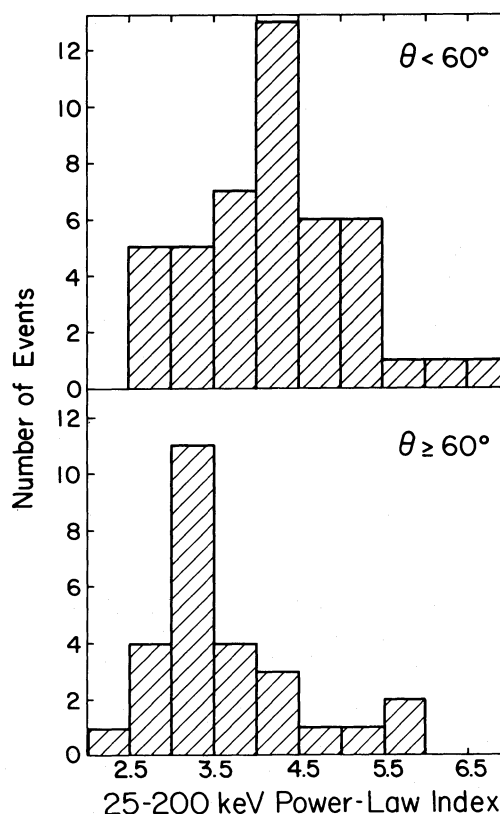

Fɪɢ. 6.—Histograms of power-law indices that provide the best fit to the *SMM* GRS measurements between 25 and 200 keV. The distributions are shown for both limb and disk samples.
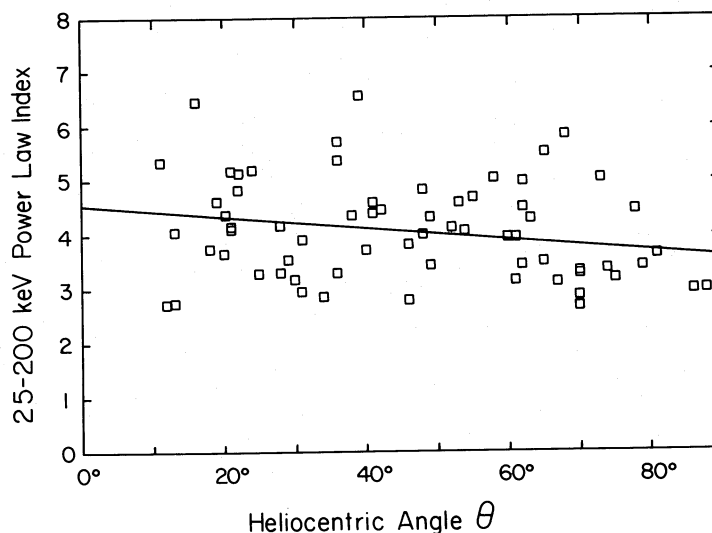
FIG. 7.—Best-fit 25–200 keV power-law indices plotted as a function of heliocentric angle. The line providing the least-squares fit is also plotted.

$\Delta p = 0.51 \pm 0.21$. When comparing the distributions, we find that the Kolmogorov-Smirnov test rejects the hypothesis that the two distributions are drawn from the same parent distribution at the 98% confidence level. In Figure 7 we have plotted the 25–200 keV spectral indices versus heliocentric angle. Also plotted is the line producing the least-squares fit, $p = 4.54(\pm 0.88) - 0.011(\pm 0.005)\theta$.

Two points are worth remembering when considering these results. First, an admixture of thermal emission must be present at these energies. Second, while the power laws used to fit the data usually work fairly well, there is no reason to expect the actual spectra to be power laws. Here we use the best-fitting power-law index only as a measure of spectral hardness.

c) Implications

The apparent spectral hardening of flares with increasing heliocentric angle is consistent with our position distribution results. To produce the observed enhancement in the number of events detected near the limb, the flux of electrons must increase as the angle with respect to the outward normal increases. Such an electron anisotropy would also produce a spectral hardening at the limb. The results are therefore qualitatively consistent with one another.

The 300 keV–1 MeV spectral results can also be compared with the 300 keV position results to check for quantitative consistency. If we assume that the radiating electrons have a downwardly directed Gaussian angular distribution and an electron injection spectrum with power-law index $s = 3.0$, then the calculations presented in Vestrand and Ghosh (1987a) indicate that the nominal half-power half-angle is $\varphi_{1/2} \sim 75°$. This half-angle is of the same order as the result from the position study.

The observed spectral variation is probably smaller than the actual bremsstrahlung spectral variation, owing to an admixture of nuclear gamma-rays. These nuclear gamma-rays are generated by the interaction of energetic ions with thermal nuclei. This nuclear component is isotropic and has a relatively flat spectrum (Chupp 1984; Ramaty, Kozlovsky, and Lingenfelter 1979). The nuclear admixture is therefore most important at the high-energy end of the 300 keV–1 MeV band in disk flares. This component tends to make the spectra of disk flares

harder than would be produced by bremsstrahlung alone. In turn, the magnitude of the apparent center-to-limb spectral variations would be smaller. This nuclear component is less important at the lower photon energies that dominate the position study.

V. VERY HIGH ENERGY EMISSION FROM FLARES

Another clue that the distribution of flare-accelerated electrons is anisotropic is available from studies of flares with emission at energies above 10 MeV. Both yield calculations (Ramaty et al. 1983) and spectral arguments (Vestrand et al. 1984) indicate that the bulk of the gamma-rays with energies greater than 10 MeV are generated by electron bremsstrahlung. The angular distribution of bremsstrahlung from a single relativistic electron is strongly directed in the forward direction (e.g., Petrosian 1985). For example, the distribution of 10 MeV photons from 30 MeV electrons reaches a maximum near the direction of the electron's velocity vector and then rapidly decreases to less than 0.001% of the maximum at angles greater than 20°. Since Compton backscattering is negligible at these energies, the anisotropy of flare radiation is significantly greater at 10 MeV than at 300 keV.

Rieger et al. (1983) have shown that the frequency distribution of flares detected at energies > 10 MeV by the SMM GRS is strongly skewed toward the limb. The positions of the 12 flares detected between 1980 February and 1986 December are shown in Figure 8. Notice that only two events occurred at heliocentric angles such that $\sin \theta < 0.9$. The fraction of limb events is therefore $f_L = 0.833$. This is significantly larger than the value $f_L = 0.391$ detected at 300 keV.

When assessing the significance of this result, one must keep an important selection effect in mind. These events were found first by the GRS flare search at 300 keV. Only after an event was found at 300 keV was the event interval searched for > 10 MeV emission. The > 10 MeV event sample will, therefore, reflect any bias that is present in the 300 keV event sample. In other words, even if the > 10 MeV emission is isotropic, one would not expect 29.5% of the events to occur at the limb. Instead one would expect the > 10 MeV events to exhibit the same enhancement toward the limb as their parent population (i.e., $\sim 39\%$ limb events). The expected number of limb events
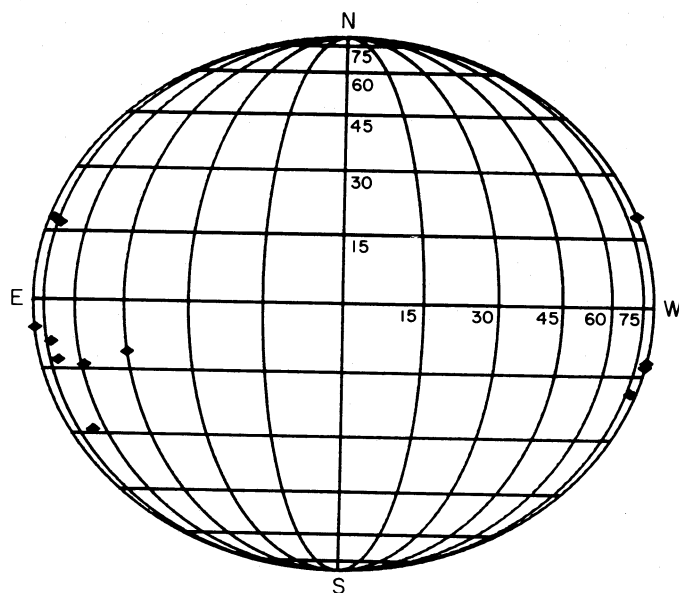
Fig. 8.—Hα positions of flares detected above 10 MeV during the period 1980 February–1982 December.

is therefore 4.7 ± 1.7. The value of 10 observed limb events therefore corresponds roughly to a 3.1 σ excess over the predicted value. This result is a bit weaker than the 4.1 σ limb enhancement that is obtained when the systematic bias introduced by the search procedure is ignored. We are presently developing an event-search procedure that will independently search for events at > 10 MeV and will therefore not be subject to this selection effect.

The potentially strong selection effect and rather poor statistics make it somewhat dangerous to draw quantitative conclusions about the energy dependence of the electron angular distribution at this point. However, if we take the limb fraction observed above 10 MeV at face value, then the electron distribution seems to be more anisotropic above 10 MeV than it is near 1 MeV. Such behavior would not be surprising if Coulomb scattering were the process controlling the angular distribution.

Nevertheless, even the more conservative analysis suggests that the emission above 10 MeV is more strongly directed than the 300 keV emission. This behavior supports the idea that the radiation directivity is produced by an electron anisotropy.

VI. DISCUSSION

In retrospect it is not surprising that earlier studies failed to find evidence for electron anisotropies. Nearly all searched for longitude variations in the frequency of X-ray flares detected at 20–50 keV. However, at these energies the broadness of the bremsstrahlung cross section coupled with strong Compton backscattering makes the emergent radiation pattern nearly isotropic even if the emitting electrons are strongly beamed. At 300 keV, where the cross sections are much more directed, evidence for electron directivity from position studies is still difficult to uncover. For example, the radiation pattern from a perfectly collimated downward electron beam generates a limb frequency enhancement of only 12% at sin θ > 0.9. For the roughly 100 events detected at these energies to date, this corresponds to only a 3 σ enhancement. When one recalls that flares are likely to have different geometries and electron direc-

tivities, it is easy to understand how electron directivity can be hidden.

Calculations have shown that at hard X-ray energies center-to-limb spectral variations are a more sensitive measure of electron directivity (e.g., Langer and Petrosian 1977; Bai and Ramaty 1978). Nevertheless, observational studies of center-to-limb spectral variations are not common. Roy and Datlowe (1975) studied spectral variations in the 17–45 keV band as a function of solar longitude for a sample of 121 solar flares detected by the *OSO 7* satellite. They concluded that there was a statistically significant softening in the spectra of events near the limb by Δp = 0.8. At first sight this result seems to be at odds with our finding that the 25–200 keV and 300 keV–1 MeV spectra harden near the limb. In fact, in a later paper Datlowe *et al.* (1977) argued that this spectral effect could not be due to anisotropy because the detection of the events at 20 keV showed no center-to-limb variation. However, these conclusion were based on calculations that did not include Compton backscattering. Bai (1977) showed that, when backscattering was included, the photon spectra below 50 keV from a downwardly directed cone of energetic electron distribution would steepen near the limb. The same distribution produced a limb hardening at energies above 100 keV.

Recently, Bogovalov *et al.* (1985) presented observations from *Venera 13* that show a center-to-limb variation in the hard X-ray spectra of flares. From a sample of 114 detected flares they refined a subsample of 37 flares that had known positions and were intense enough to allow one to derive a reliable 50–300 keV X-ray spectrum. The remaining sample of spectra showed a significant spectral hardening as the angle of observation increased. Specifically, they found a mean 50–300 keV power-law index of $p_{disk} \sim 4.3$ at $\theta < 60°$ and $p_{limb} \sim 3.2$ at $\theta > 60°$. These *Venera 13* results are qualitatively similar to the 25–200 keV results from the *SMM* GRS that are presented in § IV of this paper. However, it is difficult to compare the results quantitatively, owing to differences in the spectral energy band and the spectral unfolding technique.

Flare models can be crudely classified by whether they employ thermal emission mechanisms or nonthermal mechanisms. Thermal models assume that electrons in a given region are bulk heated to high temperatures (e.g., Chubb, Kreplin, and Friedman 1966; Brown, Melrose, and Spicer 1979). These electrons would then have a relaxed energy distribution that is a relatively efficient source of bremsstrahlung radiation. Nonthermal models assume that flare radiation is generated by the interaction of a population of nonthermal electrons with ambient cool material. The nonthermal models can be even further subdivided into thin-target and thick-target scenarios. Thin-target models assume that the radiating electrons do not lose a significant fraction of their energy before they escape the interaction region (e.g., Datlowe and Lin 1973). Thick-target models assume that all of the electron energy is lost in the interaction region (e.g., Peterson and Winckler 1959; Brown 1972; Petrosian 1973).

In the thin-target model of Datlowe and Lin (1973) hard X-rays are produced by energetic nonthermal electrons that stream radially outward through the solar atmosphere. This model predicts a disk brightened position distribution and a spectral softening at the limb. Both predictions are at odds with the *SMM* observations. On the other hand, the observed brightening and spectral hardening at the limb might be produced by predominantly horizontal streaming in a thin-target region. A constraint on the time scale for variations in this

model is set by the time required for electrons to escape from the target region. The scale height in the solar corona is $\sim 10^{10}$ cm. As a consequence, the shortest flux variations expected at 40 keV from a coronal thin-target region would be ~ 0.5 s. Thus the subsecond variations (as short as 20 ms) seen at hard X-ray energies by the *SMM* HXRBS (Kiplinger *et al.* 1983) require a chromospheric target or a significant density enhancement that is confined to a small region in the corona. Ramaty (1986) has convincingly argued that the nuclear emission detected in flares (e.g., Chupp 1984) is best explained by ion interactions in a thick target. Forrest (1983) has shown that the electron bremsstrahlung fluence is well correlated with the fluence from nuclear emission. How this correlation could arise is difficult to understand if only electron bremsstrahlung originates in a thin-target region. All together, the *SMM* GRS observations seem to indicate that the bulk of the high-energy emission in flares is not thin-target emission.

Several authors have suggested that "thermal" emission from electrons that are bulk heated to temperatures in excess of 10^8 K could be responsible for the hard X-ray emission from flares (e.g., Chubb, Kreplin, and Friedman 1966). The mean free path for particles with these energies is so large that the electrons would essentially freely stream from the source region. To avoid an extremely rapid cooling of the plasma by thermal conduction and convection into the cooler ambient plasma, Brown, Melrose and Spicer (1979) have suggested that the free-streaming electrons could generate ion-acoustic turbulence. This turbulence would in turn enhance the electron scattering rate. As a consequence, the electron velocity distribution and the resultant radiation pattern will be essentially isotropic. The relatively large anisotropy we find at > 300 keV rules out the "thermal" model in its simplest form at these energies. Of course, a directed distribution of streaming high-energy electrons may be generated by leakage or precipitation from the bulk energized source. Downwardly streaming electrons could then interact with cooler material in the atmosphere and produce the observed anisotropy. This component would then comprise a nonthermal admixture.

The simplest explanation of the *SMM* GRS observations is that the emitting electrons are accelerated in the corona and subsequently stream downward or are precipitated into a thick-target emission region lower in the atmosphere. To produce the observed limb brightening, one needs an electron distribution in the emission region that has an intensity which increases with angle from the outward normal. Likely distributions that meet this requirement are "pancake" distributions which have peak intensities in directions tangent to the photosphere (Dermer and Ramaty 1986) and downwardly directed Gaussian distributions (Vestrand and Ghosh 1987a). Dermer and Ramaty (1986) have argued that a "pancake" distribution is expected if the electrons mirror in magnetic loops. A Gaussian distribution is expected if multiple Coulomb scattering determines the angular distribution.

If one assumes that the electron angular distribution is a downwardly directed Gaussian, then the observed limb enhancement is best fitted by a Gaussian with a half-power half-angle $\varphi_{1/2} \sim 75°$. The magnitude of the center-to-limb spectral variations observed between 300 keV and 1 MeV are also best fitted by a Gaussian with a half-power half-angle $\varphi_{1/2} \sim 75°$. It is encouraging that these two different methods of assaying electron directivity give roughly the same results.

In this picture transport phenomena can play a major role in determining the angular distribution of particles that reach the target region. For example, magnetic mirroring or wave-particle scattering may play an important role in scattering particles. Since observations of the radiation directivity only give us a measure of the electron anisotropy in the target region, we cannot constrain the angular distribution produced by the accelerator without a systematic study of possible propagation effects. Such a study is beyond the scope of this work.

Electron directivity has important implications for attempts to derive the flux and spectra of energetic electrons from high-energy photon observations. Since anisotropic electron distributions can produce the photon fluxes and spectra that are strongly dependent on viewing angle, naively assuming that the radiation is isotropic can lead to significant errors in the derived fluxes and spectra of radiating electrons. In the case of downwardly directed electron distributions the energy content in high-energy electrons can be grossly underestimated. Dermer and Ramaty (1986) have pointed out that these corrections for anisotropy could make the actual electron-to-proton ratio in flares comparable to the values measured in interplanetary space. However, since there is evidence that the particle fluxes accelerated during the impulsive phase of flares are not correlated with the fluxes measured in interplanetary space (Cliver *et al.* 1983), it is not clear that such a correction is necessary. In fact, there is tantalizing evidence from observations of the 1982 June 3 flare that another type of acceleration occurs that may be responsible for the particles observed in interplanetary space (Vestrand *et al.* 1984; Forrest *et al.* 1986; Murphy, Dermer, and Ramaty 1987).

The statistical technique employed in this study is of very limited use in determining the anisotropy of electrons in an individual flare. Flaring regions are unlikely to have identical geometries. Furthermore, even within a single flare there is no guarantee that the electron anisotropy is time-independent. A promising method for measuring individual flares is the stereoscopic method first used by Catalano and Van Allen (1973). The idea is to compare simultaneous observations by spacecraft at markedly different viewing angles. Comparison of intensity versus time observations from these spacecraft can not only yield radiation directivity measurements for individual flares but also measure the time dependence of the directivity within a given event. The promise and limitations of this technique have recently been examined by Vestrand and Ghosh (1987b). That study concludes that stereoscopic observations can most easily assay the electron anisotropy in the radiation bands 300–700 keV and 10–50 MeV. In simulating stereoscopic observations by an Earth-orbiting satellite and a Sun-orbiting satellite that is located at random phase in the ecliptic plane, it was found that in a sample of 100 events one can expect to find flux ratios as large as 3 or 4 in the 300 keV band and as large as ~ 6 in the 10 MeV band if the electron distribution has a half-angle $\varphi_{1/2} \sim 75°$. If the typical half-angle is as large as $\varphi_{1/2} \sim 90°$, as permitted by the observations in this paper, then the flux ratios in the 300 keV band are typically less than ~ 2. These simulations assume that the ideal detectors on the two spacecraft are identical. Measurements by real detectors on separate spacecraft will have uncertainties due to statistical errors, to an imperfect knowledge of the response function, and to nonuniqueness of spectral unfolding (Fenimore, Klebesadel, and Laros 1983). Of course, if a type of isotropic emission is found that has an intensity which is always proportional to the energetic electron concentration, one could use observations from a single spacecraft to measure the electron directivity.

VII. CONCLUSIONS

We have examined the properties of high-energy emission from flares detected by the gamma-ray spectrometer on the *Solar Maximum Mission* satellite for indications of radiation directivity. Our principal conclusions are the following:

1. The fraction of gamma-ray flares detected at 300 keV by the *SMM* GRS that have heliocentric angles θ such that $\sin \theta > 0.9$ is significantly higher than is expected for isotropically emitting flares. We find a 2.5 σ excess in f_L for gamma-ray flares over the value predicted by Monte Carlo simulation. The excess in f_L for gamma-ray flares over the values observed for the HXRBS and Hα control groups are greater than 3 σ.

2. The spectral index distributions for limb and disk gamma-ray flares are significantly different. The power laws that provide the best fit to the data between 300 keV and 1 MeV are flatter for limb flares than for disk flares. Specifically, flares that occur at $\theta > 60°$ have a mean spectral index that is harder than flares at $\theta < 60°$ by $\Delta p = 0.37 \pm 0.11$.

3. The 25–200 keV spectra measured during the impulsive phase by the *SMM* GRS show a significant center-to-limb variation. Hard X-ray flares that occur at $\theta > 60°$ have a mean power-law spectral index that is harder than that of flares at $\theta < 60°$ by $\Delta p = 0.51 \pm 0.21$.

4. The position distribution of flares detected at > 10 MeV by the *SMM* GRS appears to be highly anisotropic. Of the 12 flares detected at energies > 10 MeV between 1980 February

and 1986 February, only two occurred at positions such that $\sin \theta < 0.9$.

5. A reinterpretation of an earlier spectral study by Datlowe *et al.* (1977) suggests that the signature of anisotropic electrons may be present even at photon energies below 40 keV.

6. These observations are at odds with the predictions from fully thermal models or thin-target nonthermal models. Their simplest interpretation is that the high-energy continuum > 300 keV is thick-target bremsstrahlung produced by an electron intensity distribution which increases with angle from the outward normal. Two families of candidate distributions are (*a*) "pancake" distributions which have peak intensities in directions parallel to the photosphere and (*b*) downwardly directed Gaussian distributions. During the impulsive phase this nonthermal component is visible down to at least 40 keV.

7. A prediction of the anisotropic bremsstrahlung interpretation is that disk flares should be richer in nuclear emission than limb flares. If one assumes that the flare radiates isotropically at energies > 300 keV, this electron anisotropy can lead to significant underestimates in the total number and spectral hardness of radiating electrons.

APPENDIX A

ATTENUATION OF BEYOND-THE-LIMB EMISSION

Suppose that an emission region is at a height h' above the photosphere and ξ radians beyond the limb. From Figure 9 we find the relationships

$$R_\odot + h'' = (R_\odot + h') \cos \xi \tag{A1a}$$

and

$$h'' = h' \cos \xi - R_\odot (1 - \cos \xi) , \tag{A1b}$$

where $R_\odot$ is the solar radius and h'' is the impact parameter of the trajectory. If we let x measure the distance along the line of sight from its intersection with h'', then the height h of the trajectory in the atmosphere is given by

$$h(h + 2R_\odot) = h''(h'' + 2R_\odot) + x^2 ,$$

or, neglecting small second-order terms,

$$h \approx h'' + \frac{x^2}{2R_\odot} . \tag{A2}$$

At a given energy the decreased visibility of a region is a function of the line-of-sight column density. This column density is found by integrating the number density along a trajectory from the flare to the spacecraft. Near the photosphere the number density profile can be approximated by

$$n(h) = n_0 \exp\left(-\frac{h - a}{b}\right) . \tag{A3}$$

By combining equations (A1)–(A3), we find that the column density is given by

$$
\begin{aligned}
\text{CD} &= 2 \int_0^{x_1} n_0 \exp\left(-\frac{h'' + x^2/2R_\odot - a}{b}\right) dx + \int_{x_1}^\infty n_0 \exp\left(-\frac{h'' + x^2/2R_\odot - a}{b}\right) dx \\
&= \left(\frac{\pi}{2} R_\odot b\right)^{1/2} n_0 \exp\left(-\frac{h'' - a}{b}\right)\left\{1 + \mathrm{erf}\left[\frac{x_1}{(2R_\odot b)^{1/2}}\right]\right\} \\
&= \left(\frac{\pi}{2} R_\odot b\right)^{1/2} n_0 \exp\left\{-\frac{1}{b}[h' \cos \xi - R_\odot(1 - \cos \xi) - a]\right\}\left\{1 + \mathrm{erf}\left[\frac{(R_\odot + h') \sin \xi}{(2R_\odot b)^{1/2}}\right]\right\} .
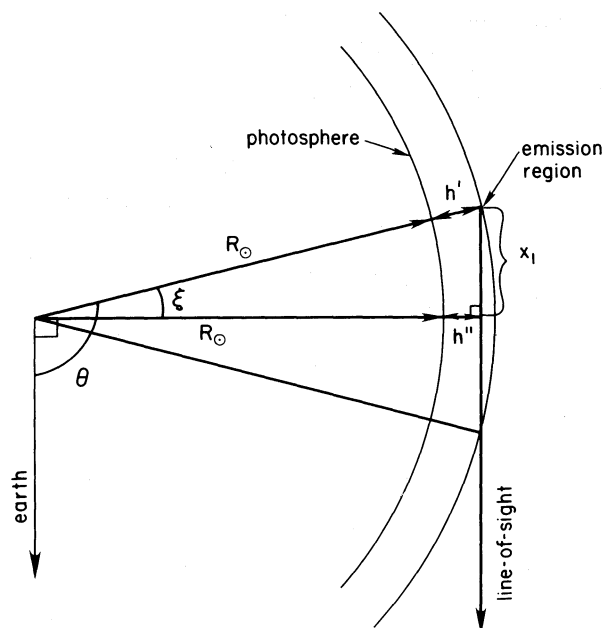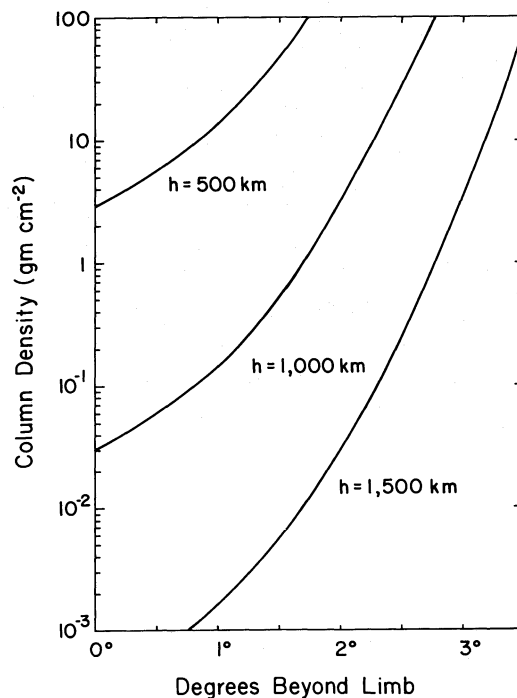\end{aligned}
\tag{A4}
$$

FIG. 9.

FIG. 10.

FIG. 9.—Geometry for an emission region that is located at a height h' above the photosphere and ξ radians beyond the limb.
FIG. 10.—Plot of column density vs. degrees beyond the limb for emission regions at heights of 5×10^2, 1.0×10^3, and 1.5×10^3 km above the photosphere.

Figure 10 shows the column density given by equation (A4) when the parameters appropriate to Allen's photospheric model (Allen 1973) are used (viz., $n_0 = 1.51 \times 10^{17}$ cm^{-3}, $b = 110$ km, $a = 0$). Notice that emission regions at less than 1500 km will be strongly attenuated even if they are only a few degrees beyond the limb.

APPENDIX B

CALCULATION OF HELIOCENTRIC ANGLES

If the radiation patterns of flares are isotropic or are cylindrically symmetric about the surface normal at the flare position, then the detectability of a flare at the Earth will be a function of its heliocentric angle. The heliocentric angle θ is defined by the angle between the Earth-Sun line and the normal to the solar surface at the flare's position. The positions of flares are listed in the NOAA *Solar-Geophysical Data* tables by average heliographic latitude, b, and average heliographic central meridian distance, l, e.g., S20 W60 ($b = -20^\circ 0$, $l = +60^\circ 0$). When the Earth's position is in the plane of the solar equator, the heliocentric angle is given by the rather simple expression

$$\theta = \arccos (\cos l \cos b) . \tag{B1}$$

A more accurate expression for heliocentric angle that includes the inclination of the solar equator to the ecliptic ($I = 7^\circ 15'$) is

$$\theta = \arccos (\sin \Delta \sin b + \cos \Delta \cos b \cos l) , \tag{B2}$$

where

$$\Delta = \arcsin [\sin (\odot - \Omega) \sin I] ,$$

$$\odot \equiv \text{Sun's position on the ecliptic} ,$$

$$\Omega = 74^\circ 48' + 52''5(t - 1980.0),$$

$$t = \text{Time expressed in years} .$$

Equation (B2) was used to calculate the heliocentric angles for flares throughout the text.

REFERENCES

Allen, C. W. 1973, *Astrophysical Quantities* (3d ed.; London: Athlone).
Bai, T. 1977, Ph.D. thesis, University of Maryland.
Bai, T., and Ramaty, R. 1978, *Ap. J.*, **219**, 705.
Bogovalov, S. V., Kel'ner, S. R., Kotov, Yu. D., Zenchenko, V. M., Vedrenne, G., Barat, C., Chambon, G., and Talon, R. 1985, *Soviet Astr. Letters*, **11**, 322.
Brown, J. C. 1972, *Solar Phys.*, **26**, 441.
Brown, J. C., Melrose, D. B., and Spicer, D. S. 1979, *Ap. J.*, **228**, 592.
Catalano, C. P., and Van Allen, J. A. 1973, *Ap. J.*, **185**, 335.
Chubb, T. A., Kreplin, R. W., and Friedman, H. 1966, *J. Geophys. Res.* **71**, 3611.

Chupp, E. L. 1984, *Ann. Rev. Astr. Ap.*, **22**, 359.
Cliver, E. W., Forrest, D. J., McGuire, R. E., and von Rosenvinge, T. T. 1983, *Proc. 18th Internat. Cosmic Ray Conf.*, **10**, 342.
Datlowe, D. W., and Lin, R. P. 1973, *Solar Phys.*, **32**, 459.
Datlowe, D. W., O'Dell, S. L., Peterson, L. E., and Elcan, M. J. 1977, *Ap. J.*, **212**, 561.
Dennis, B., Orwig, L. E., Kiplinger, A. L., Gibson, B. R., Kennard, G. S., and Tolbert, A. K. 1986, NASA TM 86236.
Dermer, C., and Ramaty, R. 1986, *Ap. J.*, **301**, 962.
Fenimore, E. E., Klebesadel, R. W., and Laros, J. G. 1983, *Adv. Space Res.*, **3**, 207.
Forrest, D. J. 1983, in *AIP Conf. Proc. 101, Positron-Electron Pairs in Astrophysics*, ed. M. Burns, A. Harding, and R. Ramaty (New York: AIP), p. 15.
Forrest, D. J., *et al.* 1980, *Solar Phys.*, **65**, 15.
Forrest, D. J., Vestrand, W. T., Chupp, E. L., Rieger, E., Cooper, J., and Share, G. H. 1986, *Adv. Space Res.*, **6**, 115.
Henoux, J. C. 1975, *Solar Phys.*, **42**, 219.
Kane, S. R. 1974, in *IAU Symposium 57, Coronal Disturbances*, ed. G. Newkirk, Jr. (Dordrecht: Reidel), p. 105.
Kane, S. R., Anderson, K. A., Evans, W. D., Klebesadel, R. W., and Laros, J. G. 1980, *Ap. J. (Letters)*, **239**, L85.
Kiplinger, A. L., Dennis, B. R., Emslie, A. G., Frost, K. J., and Orwig, L. E. 1983, *Ap. J. (Letters)*, **265**, L99.

Langer, S., and Petrosian, V. 1977, *Ap. J.*, **215**, 666.
Lehmann, E. L. 1975, *Nonparametrics: Statistical Methods Based on Ranks* (New York: McGraw-Hill), pp. 32–40.
Murphy, R. J., Dermer, C. D., and Ramaty, R. 1987, *Ap. J. (Letters)*, **316**, L41.
Peterson, L. E., and Winckler, J. R. 1959, *J. Geophys. Res.*, **64**, 697.
Petrosian, V. 1973, *Ap. J.*, **186**, 291.
———. 1985, *Ap. J.*, **299**, 987.
Ramaty, R., Kozlovsky, B., and Lingenfelter, R. E. 1979, *Ap. J. Suppl.*, **40**, 487.
Ramaty, R. 1986, in *The Physics of the Sun*, Vol. **2**, ed. P. A. Sturrock (Dordrecht: Reidel), p. 291.
Ramaty, R., Murphy, R. J., Kozlovsky, B., and Lingenfelter, R. E. 1983, *Solar Phys.*, **86**, 395.
Rieger, E., Reppin, C., Kanbach, G., Forrest, D. J., Chupp, E. L., and Share, G. H. 1983, *Proc. 18th Internat. Cosmic Ray Conf.*, **10**, 338.
Roy, J. R., and Datlowe, D. W. 1975, *Solar Phys.*, **40**, 165.
Smith, H. J., and Smith, E. V. P. 1963, *Solar Flares* (New York: Macmillan), p. 50.
Solar-Geophysical Data. 1980–1986 (Boulder: NOAA).
Vestrand, W. T., Forrest, D. J., Rieger, E., Chupp, E. L., and Share, G. H. 1984, paper presented at XXV COSPAR Meeting, Graz, Austria.
Vestrand, W. T., and Ghosh, A. 1987a, in preparation.
———. 1987b, *Proc. 20th Internat. Cosmic Ray Conf.* (Moscow), in press.

E. L. CHUPP, D. J. FORREST, and W. THOMAS VESTRAND: Physics Department, University of New Hampshire, Durham, NH   03824

E. RIEGER: Max-Planck-Institut für Extraterrestrische Physik, 8046 Garching bei München, Federal Republic of Germany

G. H. SHARE: E. O. Hulburt Center for Space Research, US Naval Research Laboratory, Washington, DC   20375